# Geosynthetic reinforced piled embankment modeling using discrete and continuum approaches

Quoc Anh Tran, Pascal Villard, Daniel Dias

▶ **To cite this version:**

Quoc Anh Tran, Pascal Villard, Daniel Dias. Geosynthetic reinforced piled embankment modeling using discrete and continuum approaches. Geotextiles and Geomembranes, 2021, 49, pp.243 - 256. 10.1016/j.geotexmem.2020.10.026 . hal-03492591

**HAL Id: hal-03492591**
**https://hal.science/hal-03492591**

Submitted on 16 Dec 2022

**HAL** is a multi-disciplinary open access archive for the deposit and dissemination of scientific research documents, whether they are published or not. The documents may come from teaching and research institutions in France or abroad, or from public or private research centers.

L'archive ouverte pluridisciplinaire **HAL**, est destinée au dépôt et à la diffusion de documents scientifiques de niveau recherche, publiés ou non, émanant des établissements d'enseignement et de recherche français ou étrangers, des laboratoires publics ou privés.

Distributed under a Creative Commons Attribution - NonCommercial 4.0 International License

Version of Record: https://www.sciencedirect.com/science/article/pii/S0266114420301357
Manuscript_eb2c6ed24b03f0fb1c771a8c632f8077

# GEOSYNTHETIC REINFORCED PILED EMBANKMENT MODELING USING DISCRETE AND CONTINUUM APPROACHES

Quoc Anh Tran, Postdoctoral scholar

*Department of Civil and Environmental Engineering, Norwegian University of Science and Technology, Norway*

Pascal Villard, Professor

*Univ. Grenoble Alpes, CNRS, Grenoble INP, 3SR, F-38000 Grenoble, France*

Daniel Dias, Professor

*Univ. Grenoble Alpes, CNRS, Grenoble INP, 3SR, F-38000 Grenoble, France*

*Antea Group, Antony, France*

**Corresponding author:**

Daniel Dias

Professor

3SR Laboratory, Grenoble Alpes University

Bâtiment Galilée, 1270 rue de la Piscine

38400 St-Martin-d'Hères

France

Phone : +33 4 76 82 79 31

Email : daniel.dias@univ-grenoble-alpes.fr

© 2020 published by Elsevier. This manuscript is made available under the CC BY NC user license
https://creativecommons.org/licenses/by-nc/4.0/

**ABSTRACT**

Understanding the load transfer mechanism can support engineers having more economical design of geosynthetic reinforced piled embankments. This study aims to investigate the load transfer mechanisms by two different numerical methods including the Discrete Element Method (DEM) and the Finite Difference Method (FDM). The DEM model adopts (a) discrete particles to simulate the micro-structure of the granular materials and (b) coupled discrete element – finite element method (DEM-FEM) to capture the interaction between granular materials and geotextiles. On the other hand, the FDM model uses an advanced constitutive soil model considering the hardening and softening behaviour of the granular materials. The numerical results show that the geotextiles can only contribute to the vertical loading resistance in cases where the soils between piles are soft enough. In terms of design, an optimum value of the geotextile tensile stiffness can be found considering the load, the soft soil stiffness and the thickness of the embankment. Both the DEM and the FDM show that a high geotextile tensile stifness is not required since an extra stiffness will slightly contribute to the efficiency of the geosynthetic reinforced piled embankments. Nevertheless, both models are useful to optimize the design of geosynthetic reinforced piled embankments.

**KEYWORDS**: Discrete Element Method; Finite Difference Method; soil arching; load transfer, reinforced piled embankment; granular embankment; softening behaviour.

# INTRODUCTION

Embankment constructions on soft soils are challenging due to potential significant settlements. Geosynthetic reinforced piled embankments are efficient to reduce soft soil settlements and the construction time compared to other soft soil improvements. To be able to do an economical design of geosynthetic reinforced piled embankments, it is required to understand the load transfer mechanisms of granular materials. However, these mechanisms are complex. Several analytical solutions were developed in former studies to quantify the reinforcement efficacy (proportion of the embankment loading onto piles) including frictional models (Terzaghi, 1943), fixed-arch models (Carlsson, 1987; Chevalier, et al., 2010) or equilibrium models (Gourc & Villard, 2000; Briancon & Villard, 2008; Huckert, et al., 2016) with different interpretations of the stress distribution on the granular embankment including the Hewlett and Randolph model (1988), Zaeske model (Zarske, 2001) or Van Eekelen model (2013; 2015).

To investigate these complex soil mechanisms, numerical models are suitable. Continuum models such as the Finite Difference Method (FDM) (Jenck, et al., 2007; Nunez, et al., 2013; Tran, et al., 2019; Briancon, et al., 2015) or Finite Element Method (FEM) (Hassen, et al., 2009; Okyay & Dias, 2010; Villard, et al., 1999) are commonly used to explore the load transfer mechanisms. The continuum models are more accessible for engineering practice and permit to easily do a full-scale simulation of geosynthetic reinforced piled embankments. However, continuum approaches rely on soil constitutive models to capture the soil mechanical properties of the granular materials. On the other hand, Discrete Element Method (DEM) can naturally capture the complex mechanical properties of granular materials. Although often limited to academic works, DEM is also well adapted to investigate the load transfer mechanisms (Chevalier, et al., 2008; Chevalier, et al., 2012; Rui, et al., 2016).

Although both continuum models and DEM models are extensively used to investigate the load transfer mechanisms in geosynthetic piled embankments, the major differences between the numerical performance of these models are not often presented. This research aims to investigate the load transfer mechanism using both the DEM and FDM models. By using adequate micro-parameters and assemblies of particles of various shapes, the DEM can naturally capture the density dependence, pressure dependence and the shear strength degradation. These parameters play a crucial role in the load transfer evolution. In FDM, the soil behaviour is restored by using a constitutive model able to simulate the soil hardening and softening. For the DEM model, to better capture the interaction between the granular material and geotextile, a coupled DEM-FEM model (Le Hello & Villard, 2009; Villard, et al., 2009) was developed in which the granular materials (particles in DEM) interact with geotextiles (finite elements which can only sustain tensile forces). In this study, three types of soil are considered including low, medium and dense granular materials. To allow the comparison between the two numerical models, the macro-parameters of the continuum model were calibrated using triaxial test results in order to reproduce the DEM ones. The numerical results reveal the insight of the load transfer mechanism and highlight the advantages and limitations of both numerical models.

# NUMERICAL MODEL OF REINFORCED PILED EMBANKMENT

## Geometry of the numerical model

The continuum model (FDM) is performed using the software FLAC3D (2011). The geosynthetic reinforced piled embankments in both FDM and DEM models include (1) piles and pile caps installed into the soft soil, (2) the granular embankment and (3) the geotextiles. We focus on investigating the load transfer mechanism in the embankment, therefore, the soft soil and the piles (0.6m diameter) are modelled by an elastic model with a distance between piles of

3m (s=3m). Due to the symmetry, only a quarter of the geosynthetic reinforced piled embankment is modelled (see Figure 1). The height of the embankment is variable for the parametric studies. To optimize the time of numerical calculation, the soft soil thickness was only 1m in the FDM model while elastic springs were used in the DEM model. The DEM and FDM models are respectively shown in Figure 2 and Figure 3.

**Figure 1 Schematic geometry of the numerical model**

**Figure 2 DEM model of geosynthetic reinforced piles embankment**

**Figure 3 FDM model of geosynthetic reinforced piles embankment**

## Numerical model of the geosynthetic reinforced granular embankments

*DEM parameters for the granular materials*

To investigate the influence of the granular materials porosity on the load transfer mechanism, three different types of soils materials are considered, denoted as loose granular (L), medium granular (M) and dense granular soils (D) (see the parameters in Table 1). Kozicki *et al.* (2014) showed that clustering particles (overlapped clumped spheres) can mimic realistic grain shapes and replicate the mechanical behaviours of granular materials. In this study, the angularity (distance between centroid of two clumped spheres) is taken as 0.8D (where D is the diameter of a single sphere) with the diameter of the spheres distributed from 0.01m to 0.04m. The DEM particles can move freely in all directions (3 degrees of freedom in translation) and in rotations (3 degrees of freedom in rotation). The DEM model was validated with experimental results (Salot, et al., 2009). They succeeded to replicate the real behaviour of granular materials considering triaxial tests. They showed that the influence of DEM particle in macroscopic behavior is slight if the number of particles is higher than 8000. Moreover, Sibille *et al.* (2019) showed that DEM, calibrated on the base of triaxial results, can well reproduce the numerical behavior of granular material under complex load paths such as geosynthetics piled embankment. Therefore, we performed series of triaxial tests with the DEM

micro parameters under three different confining pressures (10kPa, 20kPa and 30kPa). The triaxial test sample (8000 particles) is generated using the radius expansion with decrease of friction process (Chareyre and Villard, 2005). To calibrate the macro-parameter from micro-parameter, we applied the Mohr Coulomb circle method to obtain the peak and critical state friction angle from the triaxial test. The pressure dependent parameter *m*, is obtained in the graph log(E) – log($\sigma_3/p_{ref}$) ( see Figure 4) where E is the initial Young modulus, $\sigma_3$ is the confining pressure in a triaxial test and $p_{ref} = 100$ kPa is the reference pressure. Table 2 gives the values of the macro-parameters deduced from the DEM triaxial tests. The static equilibrium of the DEM simulations is reached when the ratio between the unbalance forces and the sum of contact forces is less than 0.001. (the unbalanced force is, due to dynamic effects, the difference between the load applied and the load transmitted)

The DEM geosynthetics piled embankment model was validated with the full-scale experiment (Le Hello & Villard, 2009; Villard, et al., 2016; Chalak, et al., 2019). It is not necessary to consider a numerical particles size equal to the experimental one. Indeed, based on the validated DEM model, a sufficient number of particles was selected to replicate the mechanical behavior of granular materials. In the present study, the number of particles increase proportionally with the embankment height which is respectively equal to 0.75m, 1.5m, 2.25m and 3m. It corresponds to 16000, 32000, 48000 and 64000 clumps. The number of particles by unit of volume remains the same in all simulations.

**Table 1. Micro-parameters in the DEM model for granular materials**

**Figure 4. Calibration of the pressure dependent parameter m**

**Table 2. Interpretation of the macro-parameters from the DEM triaxial tests**

*Constitutive parameters for the granular material*

While the DEM model can capture mechanical properties of the granular materials (soil hardening, shear strength degradation (softening), critical state, pressure dependent) by using a

limited number of parameters, the FDM model requires an advanced constitutive model to be able to replicate a similar behaviour. The Cap Yield model (CY soil) ~~is~~ was developed to simulate the granular soils behaviour in the software FLAC3D (2011). This constitutive model consists of a Mohr-Coulomb yield surface incorporating a cap yield surface. The hardening law was implemented for both the Mohr Coulomb shear failure criteria and cap yield surface to capture the non-linear behaviour and pressure dependent. Furthermore, the shear strength degradation (softening) was~~is~~ considered by a linear softening law coupled with the Rowe stress dilatancy formula to control the volume changes under shearing. A detailed description of the model can be found in Tran et al. (Tran, et al., 2019).

**Table 3. Macro-parameters for the FDM model**

**Figure 5. Stress–strain response with the confining pressure of 20kPa for the Loose, Medium, and Dense materials**

**Figure 6. Volumetric response with the confining pressure of 20kPa for the Loose, Medium, and Dense materials**

Table 3 presents the numerical parameters for the FDM model which were calibrated on the base of the DEM triaxial test results.

Figure 6 show the stress-strain and volumetric responses of both DEM and FDM model for the triaxial tests with a confining pressure of 20 kPa. This research is mainly focused on the load transfer mechanisms. Therefore, the parameters calibration is based on the stress-strain behaviour rather than on the volumetric behaviour. Jenck *et al.* **(Jenck, et al., 2005)** showed that the volumetric behaviour has a low influence in the load transfer mechanisms. The differences in the volumetric response can be due to the different ways used to describe the shear dilatancy. The DEM model considered the natural interlocking between particles while the FDM model is based on the Rowe stress-dilatancy formula. The elongated particle shapes in the DEM model might overestimate the soil expansion compared with the FDM model (using Rowe stress dilatancy formula) and experiment **(Salot, et al., 2009)**.

*Soft soil and pile constitutive models*

In the FDM model, the stiffness of the soft soil and piles are represented by an elastic model with an elastic modulus ($E_{def}$) and a Poisson's ratio (v). Similarly in the DEM model, the piles and soft soil layers were modeled by using elastic springs with an oedometric modulus ($E_{oed}$). Because of the different types of definition, the elastic modulus and the oedometric modulus are correlated by using Poisson's ratio by:

$$E_{oed} = \frac{E_{def}}{\beta} \tag{1}$$

$$\beta = 1 - \frac{2v^2}{1 - v} \tag{2}$$

For the sensitivity analysis, differents values of the oedometric modulus were considered (from 0.05 MPa to 1 MPa). Han *et al.* (2002) showed that if the pile stiffness is 1000 times higher than the soft soil one, the pile stiffness will not have an effect on the settlement and on the load transfer. Therefore, the oedometric modulus was fixed to 2000 MPa to eliminate the pile stiffness effect.

*Geotextiles in the DEM model: coupling between FEM (geotextiles) x DEM (granular materials)*

In the DEM model, geotextiles are modelled by triple-node triangular elements (Villard & Giraud, 1998) jointed together to form a plane continuous sheet. The geosynthetic model was validated in simple cases (Villard & Giraud, 1998) and by comparison with experimental results of laboratory tests and full-scale experiments (Villard, et al., 2000; Gourc & Villard, 2000).

For each triple-node finite element, the nodal forces are calculated from the nodal displacements as follows:

$$\{\vec{F}\} = [K_u]\{\vec{u}\} + \{\vec{F_u}\} \quad (3)$$

where: $\{\vec{F}\}$ are forces acting on the nodes; $[K_u]$ the elementary matrix of rigidity, $\{\vec{F_u}\}$ the corrective vector force resulting from the large displacement formulation and $\{\vec{u}\}$ the nodal displacements. The elementary matrix of rigidity permits to considers of the fibrous nature of the geotextile as for example the reinforcement yarns (no isotropic linear elastic material). In this paper, two perpendicular fibre directions were considered to mimic the nature of the geotextiles used in piled reinforced embankments. In the coupled DEM-FEM model, the geotextile can shear on pile but is tied to the boundary limit due to symmetry. Therefore, the friction angle between geotextile and the pile is equal to 31.5° and it allows horizontal relative displacements between piles and the geosynthetic sheet. It is thus possible to model large displacements and stretching of geosynthetic without any flexional resistance. The interaction between the particles of the granular embankment and the finite elements of the geotextile is respectively controlled by the normal and tangent forces $\{\vec{F_n}\}$ and $\{\vec{F_t}\}$. The contact laws are defined as follow:

$$\{\vec{F_n}\} = k_{ni}\{\vec{U_n}\} \quad (4)$$

$$\frac{d(\vec{F_t})}{d\vec{U_t}} = k_{ti} \text{ with } |\vec{F_t}| \leq |\vec{F_n}|tg(\delta) \quad (5)$$

where $k_{ni}$ and $k_{ti}$ are the interface normal and tangential stiffnesses respectively and $\delta$ the interface friction angle. $\vec{U_n}$ and $\vec{U_t}$ are respectively the normal overlap and the tangential relative displacement between two elements.

**Figure 7 Interaction between the geotextile finite elements and soil discrete particles (the simulations only use the clump of 2 particles, Villard *et al.* 2009)**

*Geotextile in the FDM model*

In FLAC3D, the geotextile is modelled by an isotropic linear elastic material with E is the Young's modulus and t is the thickness of the geotextile. A Poisson's ratio equal to 0.3, similar to the studies of Han and Gabr (2002), Liu et al. (2007), (Tano, et al., 2016; Tano, et al., 2017; Girout, et al., 2014) and Pham et al. (2018) is considered. For comparison, two types of elements ('liner' and 'geogrid' elements) are compared in this study. Both elements are used to model the geotextiles. They contain a soil-structure interface on both sides. The main difference is that the liner element has both bending and tensile resistance while the geogrid element has only tensile resistance. The model is performed in the large strain formulation in the FLAC3D.

The mechanical behavior of the FDM geotextile elements was calibrated based on the DEM model which was validated with analytical equations and full-scale experiments (Villard, et al., 2000; Gourc & Villard, 2000). In the FDM model, the thickness of the liner is fixed at 0.01m and Young's modulus was varied to match with the deflection of geotextile in the DEM model. The calibration shows that Young's modulus of geotextile elements (liner and geogrid elements) are linearly proportionally to the geotextile tensile stiffness in the DEM model (see Table 4). Commonly, it is expected that the multiplication of Young's modulus E and geotextile thickness t is equal to the geotextile tensile stiffness J. However, values of 0.6 x E x t = J were found to be the more appropriate in the FDM model to obtain results in good agreement with the DEM ones as presented in the next section.

**Table 4. Numerical calibration of geotextile in DEM and FDM model**

*Comparison of the geotextile between DEM and FDM models*

In both DEM and FDM models, the geotextile tensile stiffness is the same in both directions. The deflections of the geotextiles are compared for a simple case (only an uniform vertical

223 stress was applied to the geotextiles). To calibrate the geotextile properties between the DEM
224 and the FDM models, a sensitivity analysis was performed.

225 First, the geotextile tensile stiffness is fixed to 3000kN/m and the vertical forces are varied.
226 Both the deflections of the liner and the geogrid elements match well with the DEM results
227 (see Figure 8). However, the tensile strain in the FDM models are slightly higher than the
228 DEM model (See Figure 9) due to a singularity in the corner of the pile in the FDM model
229 (Tran, et al., 2019). The small difference of tensile strain of geotextile between the 'liner' and
230 the 'geogrid' elements may be due to the small bending resistance of the 'liner' element. For
231 the same deflection, the 'geogrid' element has only the tensile resistance while the 'liner' el-
232 ement has both tensile and bending resistance. Therefore, the tensile strain of the 'liner' ele-
233 ment is slightly higher. Secondly, we study the influence of the geotextile tensile stiffness in
234 the deflection. Both the DEM and the FDM models show a good agreement in terms of the
235 geotextile's deflection for different tensile stiffness with a surcharge of 1000 kN/m². (see Fig-
236 ure 10, Figure 11 and Figure 12). In the following section, we compared only the 'liner' ele-
237 ment in the FDM model with the DEM model to highlight the influence of the bending re-
238 sistance in the numerical results of the continuum model.

**Figure 8 Deflection of geotextile (J = 3000kN/m) with variation of vertical forces**

**Figure 9 tensile strain of geotextile (J = 3000kN/m) with variation of vertical forces**

**Figure 10 Deflection of geotextile (J = 2000kN/m, q=1000 kN/m²)**

**Figure 11 Deflection of geotextile (J = 3000kN/m, q=1000 kN/m²)**

**Figure 12 Deflection of geotextile (J = 6000kN/m, q=1000 kN/m²)**

239 ## NUMERICAL RESULTS

240 To investigate the load transfer mechanisms, a sensitivity analysis is performed. The micro-
241 parameters are given in Table 2 for the DEM model and the macro-parameters are given in
242 Table 3 for the FDM model. The comparison between the DEM model and the FDM model

will be concentrated on the efficacy changes and the vertical displacements of the geotextiles. In this study, the efficacy E is defined as the proportion of the embankment weight carried by the pile caps as follows:

$$E = \frac{P}{s^2 \gamma h_m} 100\% \quad (6)$$

where P is the forces transmitted to the pile cap, s denotes the pile centers spacing, $\gamma$ denotes the unit weight of embankment materials, and $h_m$ denotes the embankment height. To quantify a dimensionless vertical displacement rate, we define~~d~~ the shearing ratio, denoted as $d_s$, as the ratio between the maximum vertical displacement of the embankment ($y_{s\ max}$) and the embankment height as follows:

$$d_s = \frac{y_{s\,max}}{h_m} \quad (7)$$

## Effect of the porosity state of materials

The porosity represents the initial state of the materials. We consider three different types of granular materials (loos, medium, dense) in this study. Figure 13 and Figure 14 show the effect of the porosity on the maximum efficacy in the DEM and the FDM simulations. The soft soil stiffness is varied to get the maximum value of the efficacy obtained at the end of the numerical simulations~~.~~. The notations n34, n38 and n41 refer to the numerical simulations of dense, medium, and loose granular materials without geosynthetic reinforcement. The notation n34/J3000, n38/J3000 and n41/J3000 refers to dense, medium and loose granular materials respectively but reinforced by geotextiles (tensile stiffness of 3000kN/m). We showed that maximum efficacy is higher for denser materials (see Figure 13 and Figure 14). This confirms that materials with a higher shear resistance exhibit a higher efficacy embankment. Without geotextiles, the maximum efficacy increases with the increase of the embankment height. In contrast with geotextiles of 3000kN/m, the maximum efficacy is lower for higher embank-

ment. It means that when the embankment height is low (no significant load transfer within the granular soil layer), the major of the load is transferred to the pile caps through the geotextiles and negligible load is transferred to the soft soil. However, for higher embankment, a part of the loading is partially transferred to the soft soil. Hence, the proportion of the load onto piles (efficacy) reduces in the range from 70% to 90% for different granular materials.

Regarding the shearing ratio, without geotextiles, both the DEM and FDM predict shearing ratio from 0.1 to 0.2 in order to reach the maximum efficacy (see Figure 15). In contrast, with the geotextiles, the value of the shearing ratio reduces with the increase of the embankment height (see Figure 16). Furthermore, the FDM model predicts higher shearing ratio than the DEM model. Overall, the DEM and the FDM models predict a similar trend of efficacy change for the considered soil porosity variation and embankment heights.

**Figure 13 Maximum efficacy for different soil porosities in DEM model**

**Figure 14 Maximum efficacy for different soil porosities in FDM model (liner element)**

**Figure 15 Shearing ratio at maximum efficacy without geosynthetic reinforcement**

**Figure 16 Shearing ratio at maximum efficacy with geosynthetic reinforcement (liner element)**

Although the shearing ratio at maximum efficacy is similar between loose and dense granular materials, the efficacy of the dense granular is much higher than the loose granular materials. This could be explained through the force chains distribution in the DEM model. In the dense granular materials, the force chain directions act to towards the pile caps (see Figure 17) while in the loose granular materials, the force chain directions are more fluctuated (see Figure 18).

**Figure 17 Force chain in the dense granular material (porosity of 0.34)**

**Figure 18 Force chain in the loose granular material (porosity of 0.41)**

## Effect of the embankment height and soft soil stiffness

Four embankment heights are considered (0.75-m, 1.5-m, 2.25-m, and 3-m) ~~and~~ for subsoil stiffness ranging from 0 to 1MPa. The numerical results for two different materials n34 (dense granular material with porosity of 0.34) and n40 (loose granular material with porosity of 0.4) are presented in this section.

*Dense granular materials (n34)*

For dense granular materials, the peak friction angle $\phi_p$ is equal to 46° for the FDM models corresponding to porosity of 0.34 in the DEM models. The notations H0.75m, H1.5m, H2.25m and H3.0m denotes different embankment heights including 0.75m, 1.5m, 2.25m and 3m respectively. Without geotextiles, the efficacy is significantly reduced for low soft soil stiffness values for both models (see Figure 19 and Figure 20). In these cases, the load is transferred to the soft soil leading to significant settlements. In contrast, with the geotextiles, the efficacy is significantly high even for very soft soils (see Figure 21 and Figure 22). This demonstrated that geotextiles play an important role to transfer the load onto the piles instead of onto the soft soils. In both cases with and without geotextiles, the DEM and FDM models predict in a similar way that higher embankments will induce a higher efficacy in both the DEM and FDM models.

**Figure 19 Efficacy of dense materials without geotextile reinforcement in the DEM model**

**Figure 20 Efficacy of dense materials without geotextile reinforcement in the FDM model (liner element)**

**Figure 21 Efficacy of dense materials with geotextiles (J=3000kN/m) in the DEM model**

**Figure 22 Efficacy of dense materials with geotextiles (J=3000kN/m) in the FDM model (liner element)**

To highlight the role of geotextiles, the efficacy ratio is then calculated as:

$$E_{ratio} = \frac{E_{J=3000}}{E_{J=0}} \quad (8)$$

The efficacy ratio indicates the efficiency of the geosynthetic reinforcement in the piled embankment system. In the DEM model (see Figure 23), when the soft soil stiffness is higher than 0.2MPa, the efficacy ratio is close to 1. It means that the geotextiles do not contribute to the vertical loading resistance because settlements of the soft soil are too small to induce tensile forces of the geotextiles. However, when the soft soil stiffness is lower than 0.2MPa, the efficacy ratio increases significantly. Similarly, in the FDM model (see Figure 24), high values of the efficacy ratio are observed for the soft soil stiffness lower than 0.2MPa.

**Figure 23 Geosynthetic efficacy ratio of dense materials in the DEM model**

**Figure 24 Geosynthetic efficacy ratio of dense materials in the FDM model (liner element)**

In contrast, while the DEM model predicts an efficacy ratio being approximately 1 for high soft soil stiffnesses, the FDM model shows different results (efficacy ratio higher than one). This discrepancy is investigated for loose granular materials in the next section.

Regarding the surface settlement, the DEM model (see Figure 25) predicts slightly higher than the FDM model (see Figure 26). Overall, both models show higher surface settlements with the increase of the embankment height and the decrease of the soft soil stiffness.

**Figure 25 Surface settlement of dense materials in DEM model**

**Figure 26 Surface settlement of dense materials in FDM model (liner element)**

*Loose granular materials (n41)*

For loose granular materials, the peak friction angle $\phi_p$ is equal to $34^o$ for the FDM models corresponding to the porosity of 0.41 in the DEM models. There is a discrepancy between the DEM and FDM models (see Figure 27 and Figure 28). While there is a slight reduction of the efficacy in the low soft soil stiffness (as obtained for dense granular material) in the DEM model, there is no efficacy decline in the FDM model. The granular materials can dilate or densify under shearing in the DEM model and it results of soil densification. Therefore, the DEM granular materials gradually exhibit the softening behaviour leading to the reduction of

the efficacy. In contrast, for the FDM model, the materials depend on the constitutive soil model which does not considers the variation of the porosity, then, no efficacy reduction is obtained.

**Figure 27 Efficacy of loose materials without geosynthetic reinforcement in the DEM model**

**Figure 28 Efficacy of loose materials without geosynthetic reinforcement in the FDM model (liner element)**

**Figure 29 Efficacy of loose materials with geotextiles (J=3000kN/m) in the DEM model**

**Figure 30 Efficacy of loose materials with geotextiles (J=3000kN/m) in the FDM model (liner element)**

When the soft soil stiffness is low, the efficacy values for loose or dense granular materials are very high (see Figure 29 and Figure 30). It again confirms the important role of the geotextiles in the load transfer mechanisms as the geotextiles considerably increase the efficacy of the piled embankments.

**Figure 31 Geosynthetic efficacy ratio of loose materials in the DEM model**

**Figure 32 Geosynthetic efficacy ratio of loose materials in the FDM model (liner element)**

Similar values of efficacy ratio for the loose and the dense granular materials are obtained (see Figure 31 and Figure 32). In the DEM model, the efficacy ratio is approximately one while in the FDM model, the efficacy ratio ranged from 1 to 2 for high soft soil stiffnesses. In both dense and loose granular materials, the difference of the efficacy ratio between the DEM and FDM model may be due to the difference of the geotextile mechanical model. Regarding the surface settlement, the DEM model (see Figure 25) predicts slightly higher than the FDM model (see Figure 26). Overall, both models show higher surface settlements with the increase of the embankment height and the decrease of the soft soil stiffness.

In the DEM model, the geotextiles are modelled as finite element membranes able to capture the membrane effects for large displacements. The geotextiles are only involved tensile forces due to the vertical loading when their deflection is large. Therefore, a small geotextile deflec-

tion induced negligible efficacy ratio changes. In contrast, a small geotextile deflection can induce a small vertical loading resistance which may stem from the bending resistance of the 'liner' element in the FDM model, leading to the increase of the efficacy ratio. Regarding the surface settlement, both DEM and FDM model (see Figure 33 and Figure 34) show higher surface settlements of the loose material with the increase of the embankment height and the decrease of the soft soil stiffness in a similar way to the dense material. Furthermore, the settlement of the loose material is higher than the dense material in the same loading condition. Because the DEM model can capture the evolution of the porosity, there are higher settlements of the DEM model than the FDM model.

**Figure 33 Surface settlement of loose materials in DEM model**

**Figure 34 Surface settlement of loose materials in FDM model (liner element)**

**Effect of the geotextile tensile stiffness and element type in the FDM model**

To investigate the influence of the geotextile tensile stiffness, we performed simulations with different geotextile tensile stiffness (0 to 6000kN/m) for the loose and dense granular materials. Because the geotextiles are efficient when the soft soil is lower than 0.2kPa, the soft soil stiffness is fixed to 0.1MPa in all simulations to mobilize maximum efficiency of the geotextiles. The FDM elements (liner or geogrid element) used to simulate the geotextile are compared with each other.

*Dense granular materials (n34)*

Both DEM and FDM models predict a quite similar trend for dense granular materials (see Figure 35-31). The higher embankments have more efficacy for the same geotextile tensile stiffness. The efficacy increases significantly when the geotextile tensile stiffness ranges from 0 to 1000kN/m. When the geotextile tensile stiffness is higher than 1000 kN/m, the extra ten-

358 sile stiffness contributes negligibly to the efficiency of the geosynthetic reinforced piled em-
359 bankment in terms of vertical loading resistance.

**Figure 35 Effect of geotextiles tensile stiffness in the DEM model for dense granular materials**

**Figure 36 Effect of geotextiles tensile stiffness in the FDM model (liner element) for dense granular materials**

360 **Figure 37 Effect of geotextiles tensile stiffness in FDM model (geogrid element) for dense**
361 **granular materials**

**Figure 38 Efficacy versus shearing ratio in the DEM model for dense granular materials**

**Figure 39 Efficacy versus shearing ratio in the FDM model (liner element) for dense granular materials**

362 **Figure 40 Efficacy versus shearing ratio in FDM model (geogrid element) for dense**
363 **granular materials**

364 Figure 38-34 show the relation between the efficacy and the shearing ratio, computed from
365 equation (7), for different geotextile tensile stiffnesses. In both models, increasing the geotex-
366 tile tensile stiffness induce a higher efficacy and a lower geotextile deflection. In the DEM
367 model, the efficacy increases linearly with the decrease of the shearing ratio in the same way
368 regardless all studied embankment heights. A similar trend was observed for the 'geogrid' el-
369 ement in the FDM model. In contrast, for the 'liner' element in the FDM model, the efficacy
370 increases exponentially with the increase of the shearing ratio. The increase of the efficacy
371 may be due to the extra bending resistance of the 'liner' element in the FDM model apart
372 from the tension resistance of the geosynthetics elements.

373 *Loose granular materials (n41)*

374 Apart from the dense granular materials, the influence of the geotextile tensile stiffness on the
375 transfer mechanisms of loose granular materials is also investigated. Figure 41-37 show the
376 influence of the geotextile tensile stiffness for different embankment heights. A similar trend
377 in the relation between the efficacy and the geotextile tensile stiffness is observed for the
378 loose and the dense granular materials. The efficacy increases dramatically when the geotex-
379 tile tensile stiffness rises until 1000kN/m and then gradually increases for geotextile tensile

stiffnesses higher than 1000 kN/m. The relation between the efficacy and the shearing ratio is also similar between the loose and dense granular materials. -

There is a linear increase of the efficacy with the decrease of the shearing ratio in the DEM model in Figure 44 (relative similar inclination between dense and loose materials) and for the 'geogrid' element in the FDM model (see Figure 45). In contrast, there is an exponential increase of the efficacy with the decrease of the shearing ration for the 'liner' element in the FDM model (see Figure 46). This observation demonstrated that the influence trend of the geotextile tensile stiffness is independent of the porosity state of the granular materials.

**Figure 41 Effect of geotextiles tensile stiffness in the DEM model for loose granular materials**

**Figure 42 Effect of geotextiles tensile stiffness in the FDM model (liner element) for loose granular materials**

**Figure 43 Effect of geotextiles tensile stiffness (geogrid element) in FDM model for loose granular materials**

**Figure 44 Efficacy versus shearing ratio in the DEM model for loose granular materials**

**Figure 45 Efficacy versus shearing ratio in the FDM model (liner element) for loose granular materials**

**Figure 46 Efficacy versus shearing ratio in FDM model (geogrid element) for loose granular materials**

The differences between the liner and geogrid elements in the FDM model may stem from the mechanical model of the geotextile. As mentioned previously, in a high tensile stiffnesses, the 'liner' elements ~~transfers~~transfer more load to the piles due to the bending resistance under large deformation while the 'geogrid' elements and finite elements in the DEM model do not have bending resistance. Overall, the sensitivity analysis can contribute to determine the efficiency zone of the use of geotextiles (see Figure 47). In the cases study, it was demonstrated that the soil between piles should be soft enough (lower than 0.2MPa) to mobilize the vertical loading resistance of the geotextiles. This is a valuable information for engineers to design the piled embankment economically.

**Figure 47 Efficacy zone of the geotextiles**

## CONCLUSIONS

Geotextiles are effective to reinforce piled embankment systems. The load transfer mechanism plays an important role in the system efficiency. This efficiency can be given by the proportion of the load transferred onto the piles (efficacy) and the geotextile deflection. In this study, this phenomenon is investigated by two different approaches including DEM and FDM models. The DEM model adopted a granular assembly for the granular embankment and a coupled DEM-FEM for considering the geosynthetic behaviour and the interaction between the granular material and the geotextile. The conventional FDM model uses (a) an advanced constitutive soil model capable of capturing the shear strength degradation and (b) liner element or geogrid element to model the mechanical behaviour of the geotextiles. After calibration of the 'liner' and 'geogrid' element stiffness, both the DEM model and FDM models have demonstrated the capability to have better understanding of the load transfer mechanism in order to design the geosynthetic reinforced piled embankment more economically. The numerical results show that the continuum model (FDM) can overestimate the efficacy due to the extra bending resistance of the geotextiles for the 'liner' element. Consequently, the 'geogrid' element is preferable for the analysis of the geosynthetic reinforced pile embankments when the membrane effect is presented. On the other hand, the DEM model also appeared preferable as the geotextile element only considers the membrane effects with tensile strength. The efficiency of the geosynthetic reinforcement piled embankments is investigated. The geotextiles can only contribute to the vertical loading resistance when the geotextile deflection is large enough corresponding to low values of the soft soil stiffness (see Figure 47). According to numerical analyses in both DEM and FDM, the numerical optimal value of the geotextile tensile stiffness is approximately 1000kN/m for the chosen pile network geometry. An extra

tensile stiffness contributes very slightly to the efficiency of the geosynthetic reinforced piled embankments in both numerical models.

## REFERENCES


Anon., 2011. *FLAC3D Manual Version 5.0, Fast Lagrangian Analysis of Continua, Itasca Consulting Group Inc.,* s.l.: s.n.

Briancon, L., Dias, D. & Simon, C., 2015. Monitoring and numerical investigation of rigid inclusions reinforced industrial building. *Canadian Geotechnical Journal,* 52(10), pp. 1592-1604.

Briancon, L. & Villard, P., 2008. Design of geosynthetic-reinforced platforms spanning localized sinkholes. *Geotextiles and Geomembranes,* Volume 24, pp. 416-428.

Carlsson, B. O., 1987. *Reinforced soil,principles for calculation.* Linkoping, Sweden: Terratema AB.

Chalak, C., Briancon, L. & Villard, P., 2019. Coupled numerical and experimental analyses of load transfer mechanisms in granular-reinforced platform overlying cavities. *Geotextiles and Geomembranes,* Volume 47, pp. 587-597.

Chevalier, B., Briancon, L., Villard, P. & Combe, G., 2010. *Prediction of load transfers in granular layers used in rigid inclusions technique - experimental and discrete element method analysis.* s.l., s.n.

Chevalier, B., Combe, G. & Villard, P., 2008. DEM numerical analysis of load transfers in granular soil layer. *Studia Geotechnica et Mechanica,* 30(1-2), pp. 147-163.

Chevalier, B., Combe, G. & Villard, P., 2012. Experimental and discrete element modeling studies of the trapdoor problem: Influence of the macro-mechanical frictional parameters. *Acta Geotechnica,* 7(1), pp. 15-39.

448 Girout, R., Blanc, M., Dias, D. & Thorel, L., 2014. Numerical analysis of a geosynthetic-
449 reinforced piled load transferplatformeValidation on centrifuge test. *Geotextiles and*
450 *Geomembranes,* Volume 42, pp. 525-539.

451 Gourc, J. & Villard, P., 2000. *Reinforcement by membrane effect: Application to*
452 *Embankments on Soil Liable to Subsidence.* Malaysia, s.n., pp. 55-72.

453 Han, J. & Gabr, M., 2002. Numerical analysis of geosynthetic-Reinforced and Pile-Supported
454 Earth Platforms over Soft Soil. *Journal of Geotechnical and Geoenvironmental Engineering,*
455 128(1), pp. 44-53.

456 Hassen, G., Dias, D. & deBuhan, P., 2009. Multiphase constitutive model for the design of
457 piled embankment. Comparision with three.dimensional numerical simulations. *International*
458 *Journal of Geomechanics,* 9(6), pp. 258-266.

459 Hewlett, W. J. & Randolph, M. F., 1988. Analysis of piled embankments. *Gournd*
460 *Engineering,* 21(3), pp. 12-18.

461 Huckert, A., Briancon, L., Villard, P. & Garcin, P., 2016. Load transfer mechanisms in
462 geotextile-reinforced embankments overlying voids: Experimental and analytical approaches.
463 *Geotextiles and Geomembranes,* 44(3), pp. 442-456.

464 Jenck, O., Dias, D. & Kastner, R., 2005. Ground improvement by vertical rigid piles-Two-
465 dimentional physical modelling and comparison with current design methods. *Soils and*
466 *Foundation,* 45(6), pp. 15-31.

467 Jenck, O., Dias, D. & Kastner, R., 2007. Two-dimensional physical and numerical modeling
468 of a piled support earth platform over soft soil. *Journal of Geotechnical and*
469 *Geoenvironmental Engineering,* 133(3), pp. 295-305.

Kozicki, J., Tejchman, J. & Muhlhaus, H. B., 2014. Discrete simulations of a traixial compression test for sand. *International Journal for Numerical and Analytical Methods in Geomechanics,* 38(18), pp. 1923-1952.

Le Hello, B. & Villard, P., 2009. Embankments reinforced by piles and geosynthetics - Numerical and experimental studies dealing with the transfer of load in the soil embankment. *Engineering Geology,* 106(1-2), pp. 78-91.

Liu, H., Charles, W. W. N. & Fei, K., 2007. Performance of a Geogrid-Reinforced and Pile-Supported Highway Embankment over Soft Clay: Case Study. *Journal of Geotechnical and Geoenvironmental Engineering,* 133(12), pp. 1484-1493.

Nunez, M., Briancon, L. & Dias, D., 2013. Analyses of a pile supported embankment over soft clay: Full-scale experiment, analytical and numerical approaches. *Engineering Geology,* Volume 153, pp. 53-67.

Okyay, U. S. & Dias, D., 2010. Use of lime and cement treated soils as pile supported load transfer platform. *Engineering Geology,* 114(1-2), pp. 34-44.

Pham, H. V., Dias, D. & Dudchenko, A., 2018. 3D modeling of geosynthetic-reinforced pile-supported embankment under cyclic loading. *Geosynthetics International.*

Rui, R. et al., 2016. Evolution of soil arching; 2D DEM simulations. *Computers and Geotechnics,* Volume 73, pp. 199-209.

Salot, C., Gotteland, P. & Villard, P., 2009. Influence of relative density on granular materials behavior: DEM simulations of triaxial tests. *Granular Matter,* Volume 11, pp. 221-236.

Sibille, L., Villard, P., Darve, F. & Hosn, R. A., 2019. Quantitative prediction of discrete element models on complex loading paths. *International Journal for Numerical and Analytical Methods in Geomechanics,* 43(5), pp. 858-887.

493 Tano, B. F. G. et al., 2016. Numerical modeling of the nonlinear mechanical behavior of
494 multilayer geosynthetic system for piggyback landfill expansions. *Geotextiles and*
495 *Geomembranes,* Volume 44, pp. 782-798.

496 Tano, B. F. G. et al., 2017. A numerical modelling technique for geosynthetics validated on
497 acavity model test. *Geotextiles and Geomembranes,* Volume 45, pp. 339-349.

498 Terzaghi, K., 1943. *Theoretical soil mechanics.* Hoboken, NJ: Wiley.

499 Tran, Q. A., Villard, P. & Dias, D., 2019. Discrete and continuum numerical modeling of soil
500 arching between piles. *International Journal of Geomechanics,* 19(2), p. 04018195.

501 Van Eekelen, S. J. M., Bezuijen, A. & van Tol, A. F., 2013. An analytical model for arching
502 in piled embankment. *Geotextiles and Geomembranes,* Volume 39, pp. 78-102.

503 Van Eekelen, S. J. M., Bezuijen, A. & van Tol, A. F., 2015. Validation of analytical models
504 for the design of basal reinforced piled embankments. *Geotextiles and Geomembranes,*
505 Volume 43, pp. 56-81.

506 Villard, P., Chevalier, B., Le Hello, B. & Combe, G., 2009. Coupling between finite and
507 discrete element methods for modelling of earth structures reinforced by geosynthetic.
508 *Computers and Geotechnics,* 36(5), pp. 709-717.

509 Villard, P., Chevalier, B., Le Hello, B. & Combe, G., 2009. Coupling between finite and
510 discrete element methods for the modeling of earth structures reinforced by geosynthetic.
511 *Computers and Geotechnics,* pp. 709-717.

512 Villard, P. & Giraud, H., 1998. Three-dimensional modelling of the behaviour of geotextile
513 sheets as membrane. *Tex Res J,* pp. 797-806.

514 Villard, P., Gource, J. P. & Feki, N., 1999. Analysis of geosynthetic lining systems
515 (GLS)undergoing large deformations. *Geotextiles and Geomemranes,* Volume 17, pp. 17-32.

516 Villard, P., Goutce, J. & Blivet, J., 2000. A geosynthetic reinforcement solution to prevent the
517 formation of localized sinkholes. *Rev France Getechnique,* pp. 23-34.

518 Villard, P., Huckert, A. & Briancon, L., 2016. Load transfer mechanisms in geotextile-
519 reinforced embankmentsoverlying voids: Numerical approach and design. *Geotextiles and*
520 *Geomembranes,* Volume 44, pp. 381-395.

521 Zarske, D., 2001. *Zur wirkungsweise von unbewehrten und bewehrten mineralischen*
522 *tragschichten uber pfahlartigen grundungselementen,* Kassel, Germany: Schriftenreihe
523 Geotechnik.

524

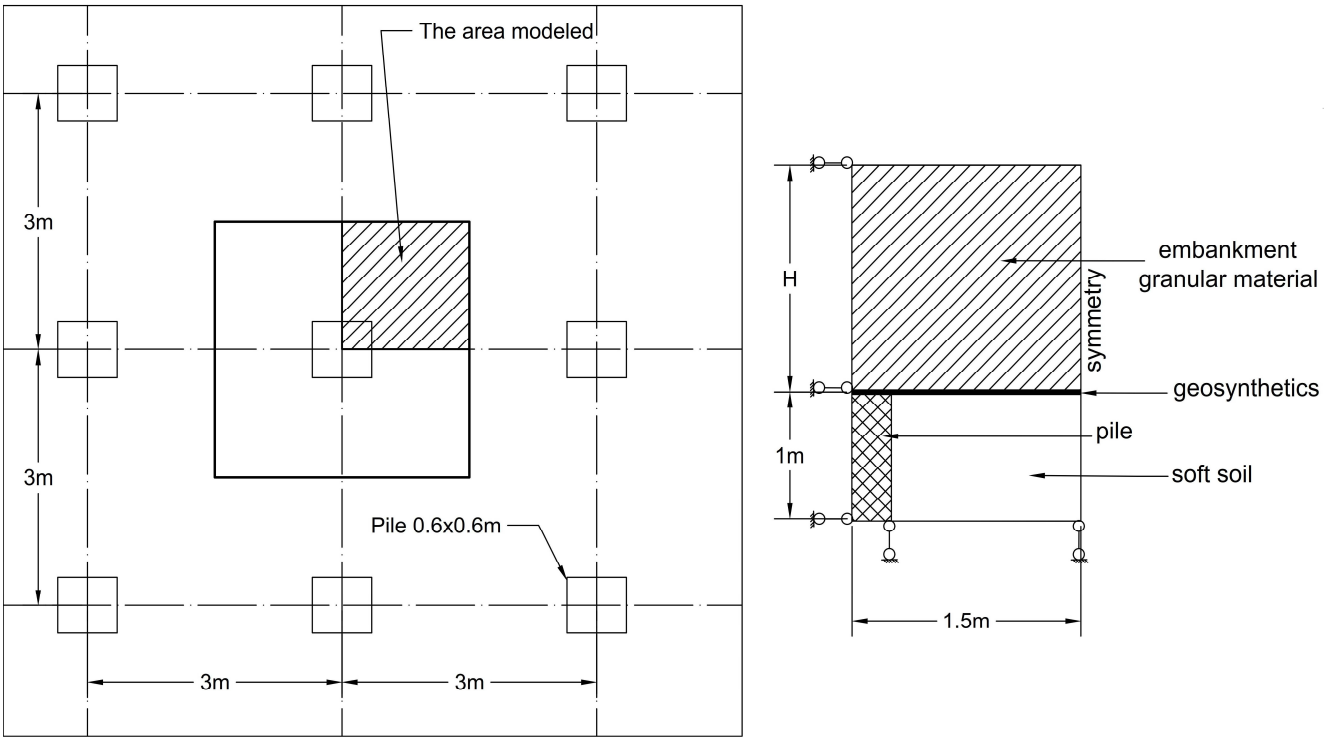


**Figure 1 Schematic of the numerical model**

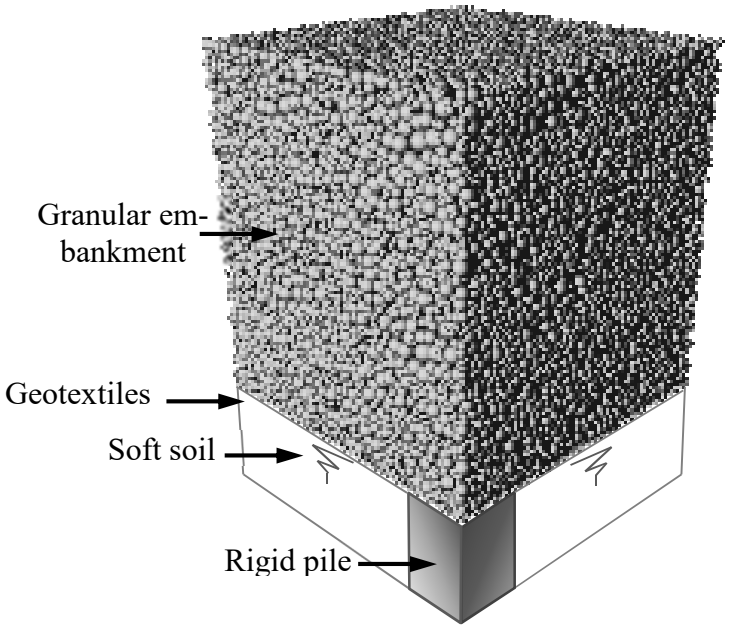


**Figure 2 DEM model of geosynthetic reinforced piled embankment**

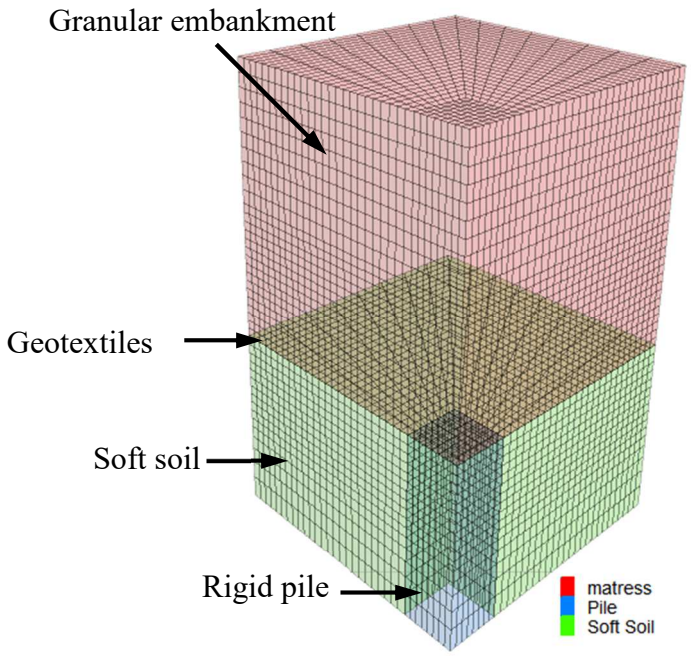


**Figure 3 FDM model of geosynthetic reinforced piled embankment**

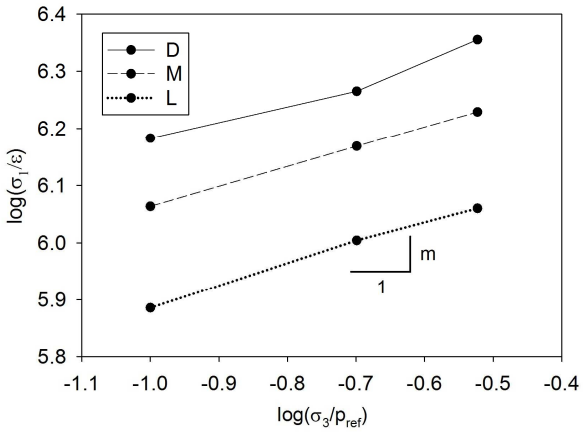


**Figure 4. Calibration of pressure dependent parameter m**

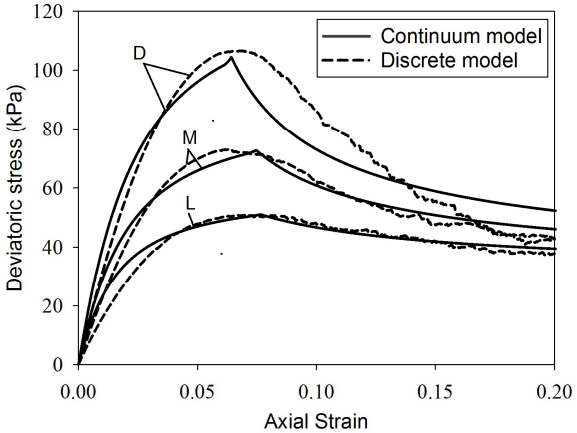


**Figure 5. Stress–strain response for the Loose, Medium, and Dense granular materials**

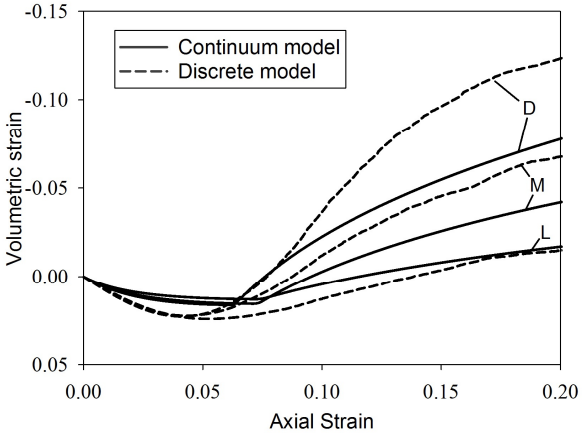


**Figure 6. Volumetric response for the Loose, Medium, and Dense granular materials**

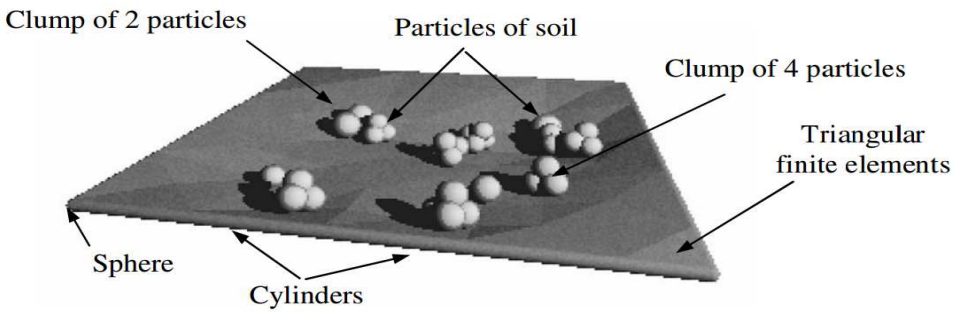


**Figure 7 Interaction between the geotextile finite elements and soil discrete particles (the simulations only use the clump of 2 particles, Villard et al. 2009)**

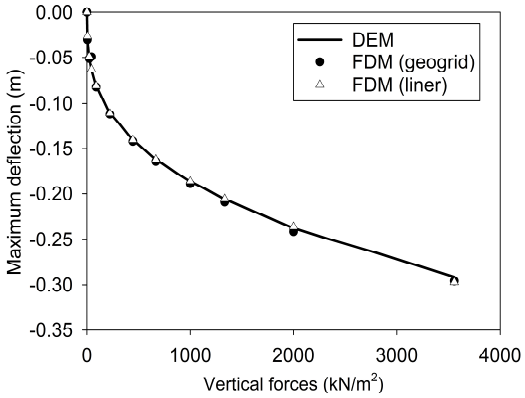


**Figure 8 Deflection of geotextile (J = 3000kN/m) with variation of vertical forces**

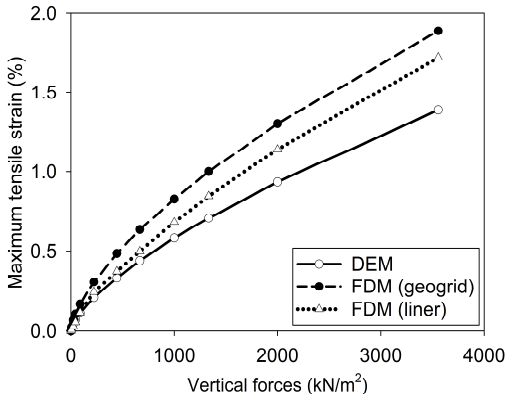


**Figure 9 tensile strain of geotextile (J = 3000kN/m) with variation of vertical forces**

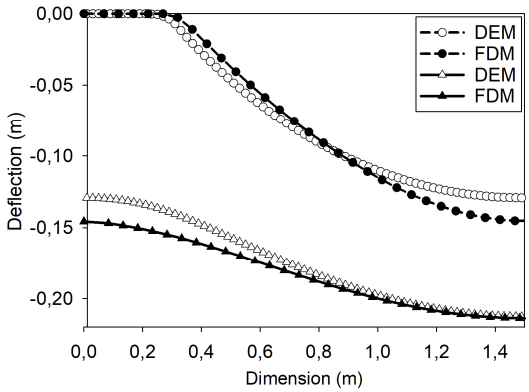


**Figure 10 Deflection of geotextile (J = 2000kN/m, q=1000 kN/m²)**

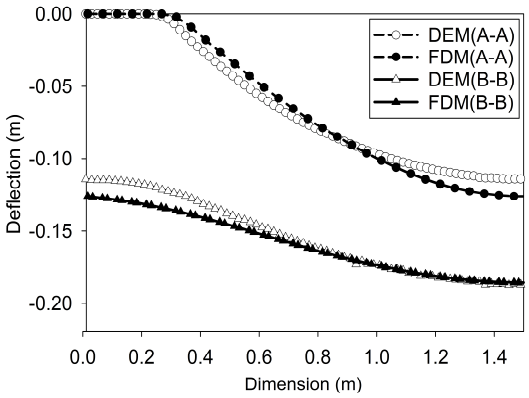


**Figure 11 Deflection of geotextile (J = 3000kN/m, q=1000 kN/m²)**

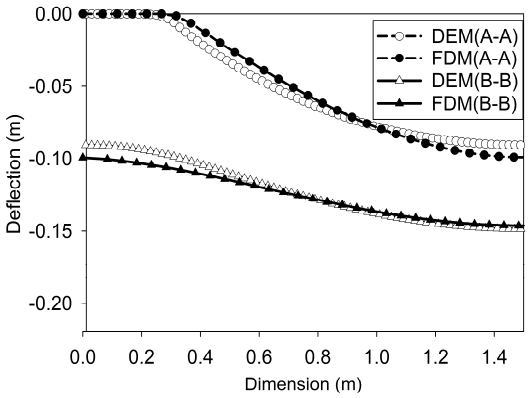


**Figure 12 Deflection of geotextile (J = 6000kN/m, q=1000 kN/m²)**

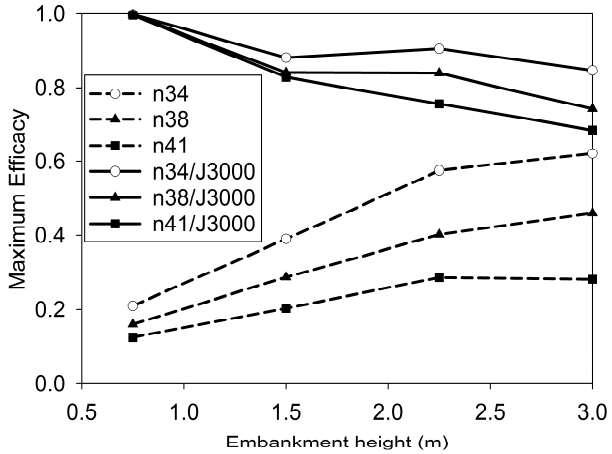


**Figure 13 Maximum efficacy for different porosity in DEM model**

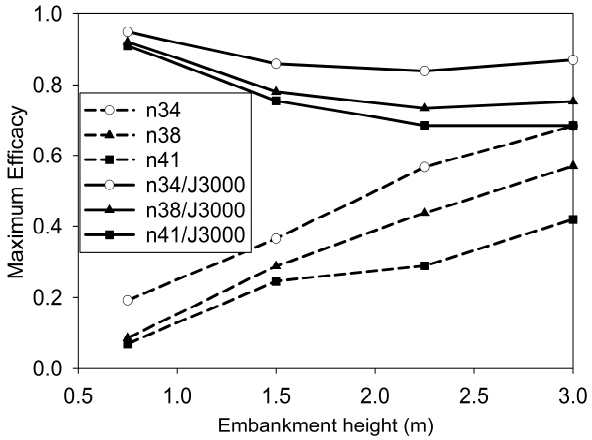


**Figure 14 Maximum efficacy for different porosity in FDM model (liner element)**

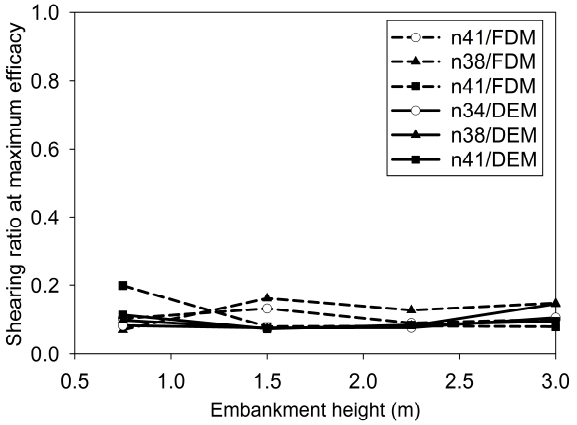


**Figure 15 Shearing ratio at maximum efficacy without geosynthetic reinforcement**

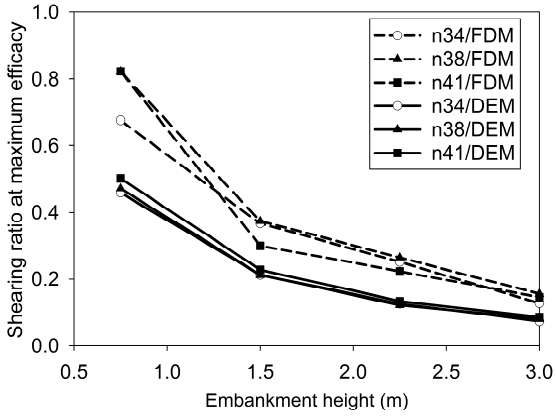


**Figure 16 Shearing ratio at maximum efficacy with geosynthetic reinforcement**

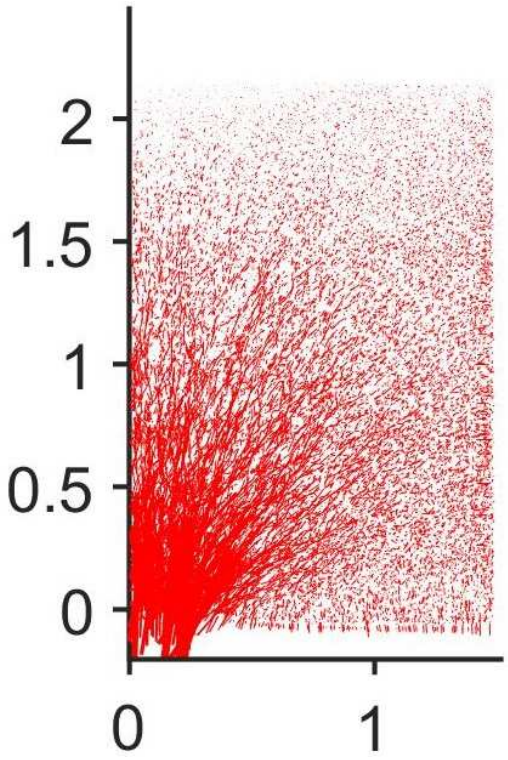


**Figure 17 Force chain in the dense granular material (porosity of 0.34)**

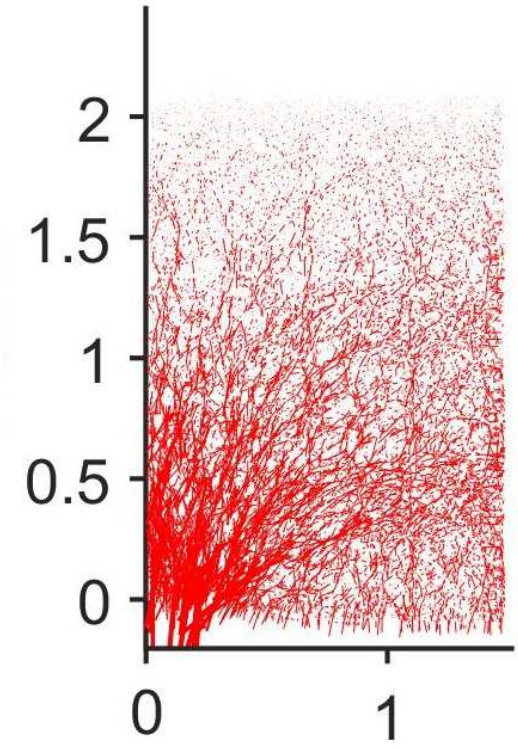


**Figure 18 Force chain in the loose granular material (porosity of 0.41)**

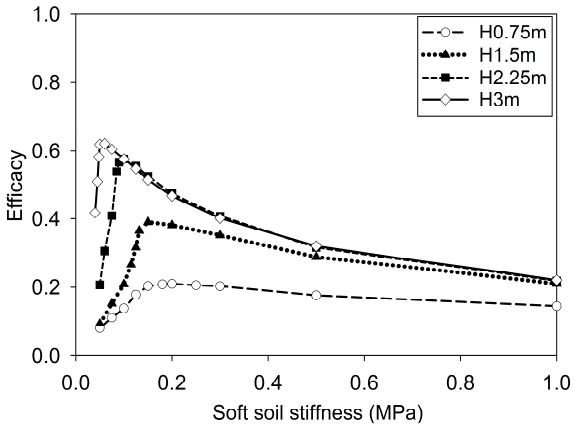


**Figure 19 Efficacy of dense materials without geotextiles reinforcement in DEM model**

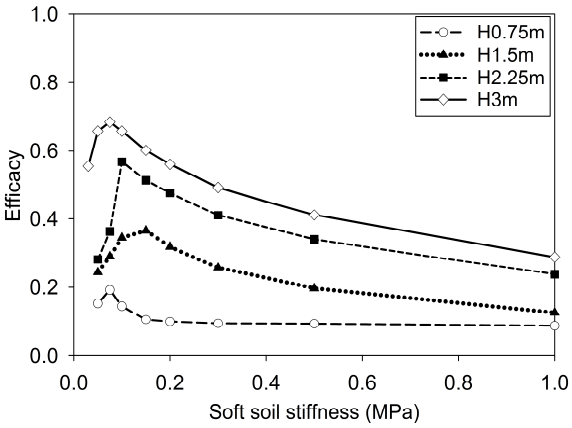


**Figure 20 Efficacy of dense materials without geotextiles reinforcement in FDM model (liner element)**

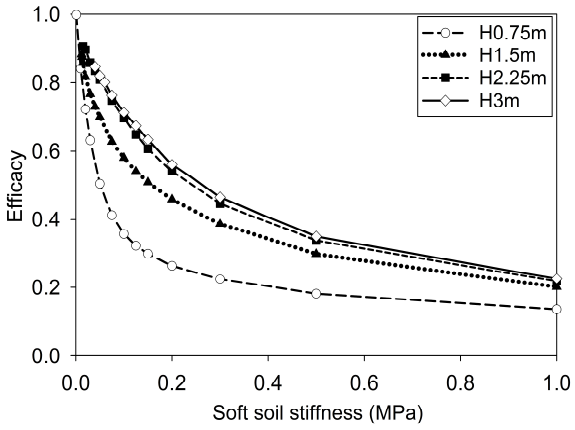


**Figure 21 Efficacy of dense materials with geotextiles (J=3000kN/m) in DEM model**

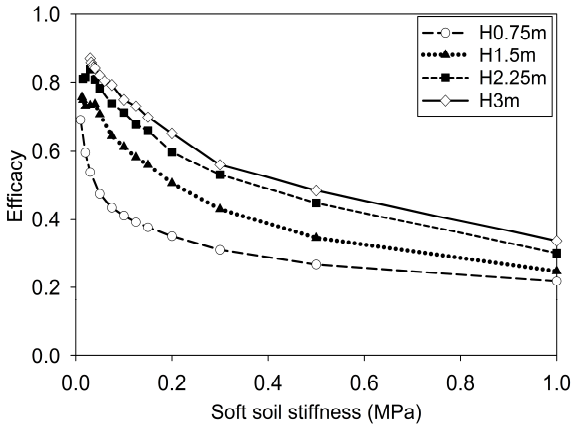


**Figure 22 Efficacy of dense materials with geotextiles (J=3000kN/m) in FDM model (liner element)**

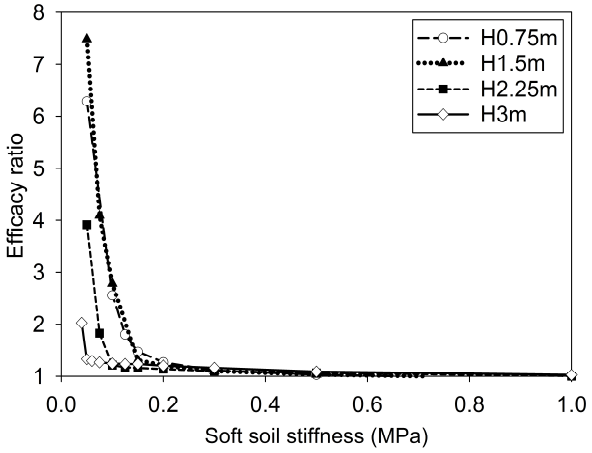


**Figure 23 Efficacy ratio of dense materials in DEM model**

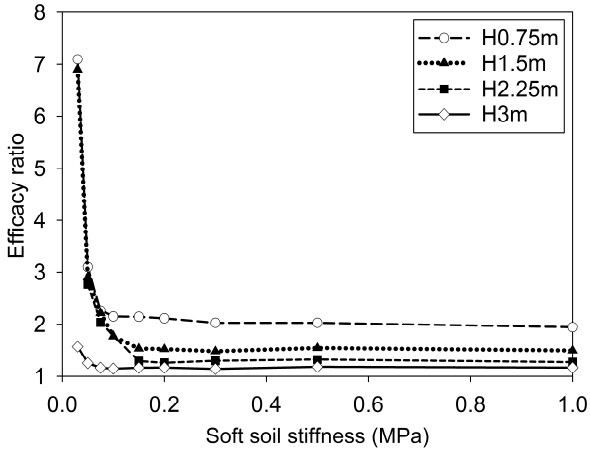


**Figure 24 Efficacy ratio of dense materials in FDM model (liner element)**

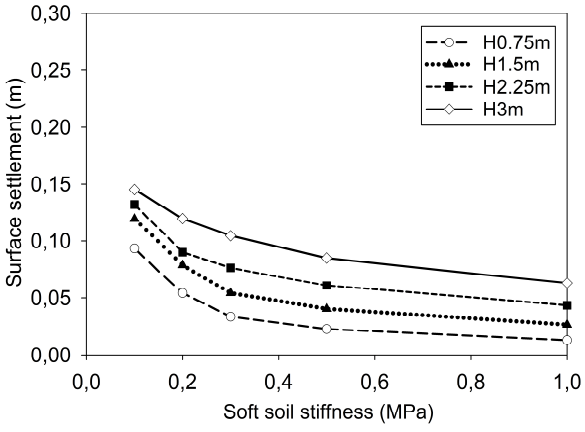


**Figure 25 Surface settlement of dense materials in DEM model**

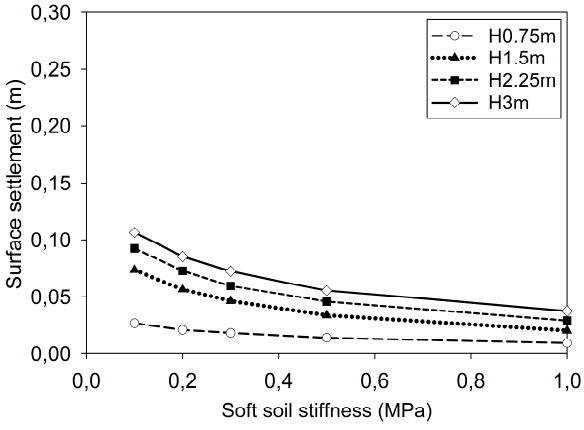


**Figure 26 Surface settlement of dense materials in FDM model (liner element)**

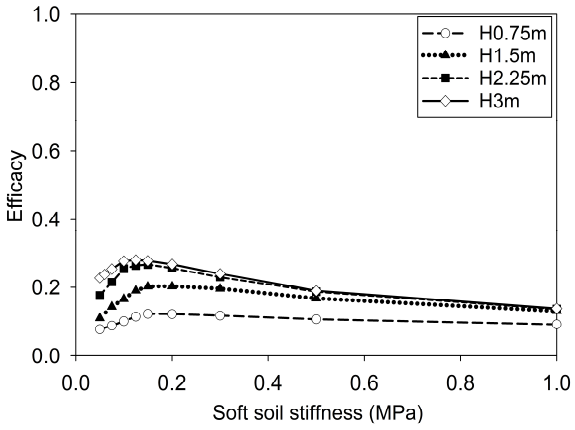


**Figure 27 Efficacy of loose materials without geosynthetic reinforcement in DEM model**

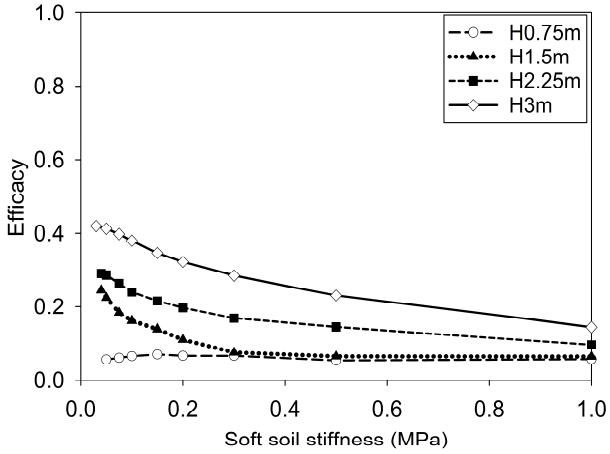


**Figure 28 Efficacy of loose materials without geosynthetic reinforcement in FDM model (liner element)**

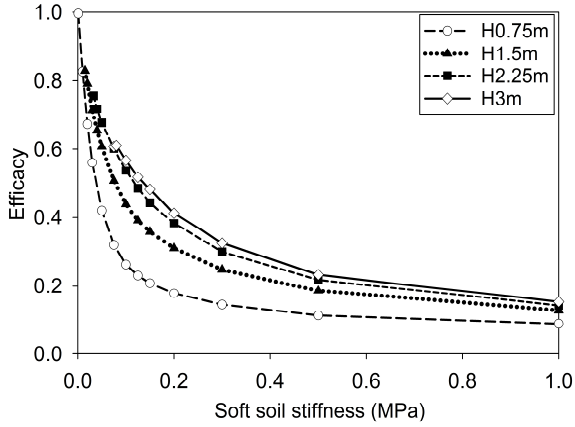


**Figure 29 Efficacy of loose materials with geosynthetic reinforcement in DEM model**

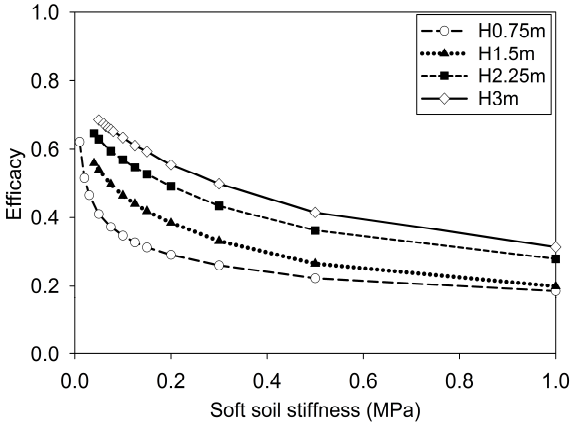


**Figure 30 Efficacy of loose materials with geosynthetic reinforcement in FDM model (liner element)**

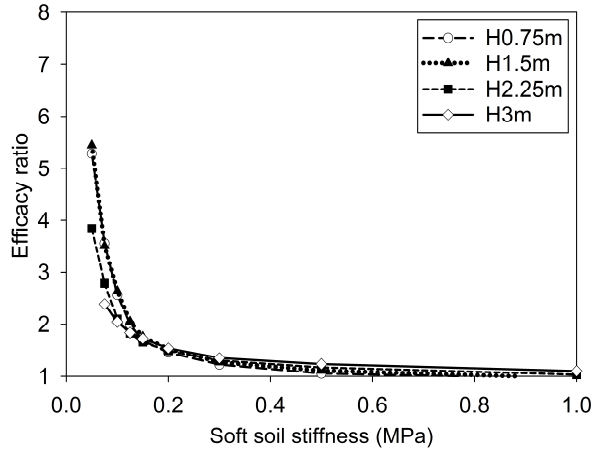


**Figure 31 Efficacy ratio of loose materials in DEM model**

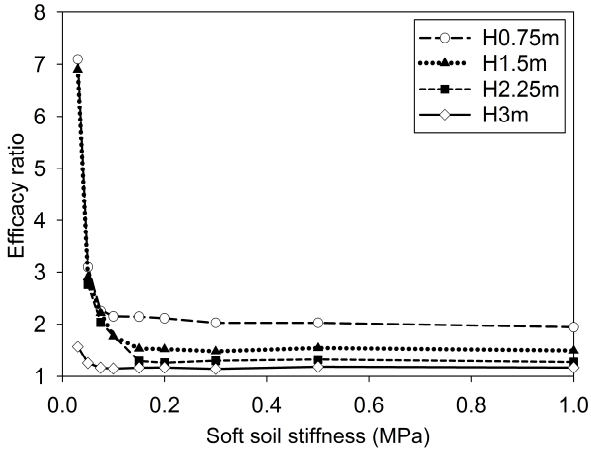


**Figure 32 Efficacy ratio of loose materials in FDM model (liner element)**

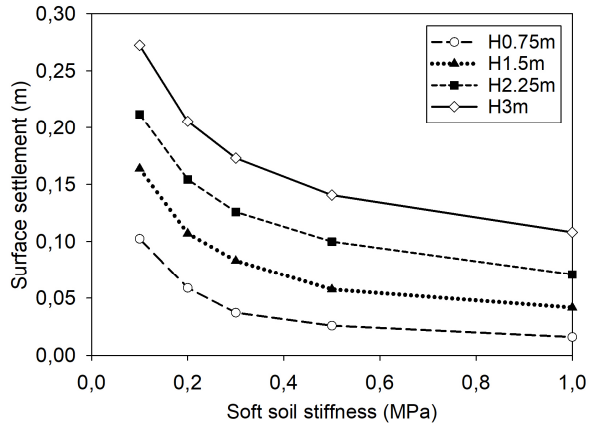


**Figure 33 Surface settlement of loose materials in DEM model**

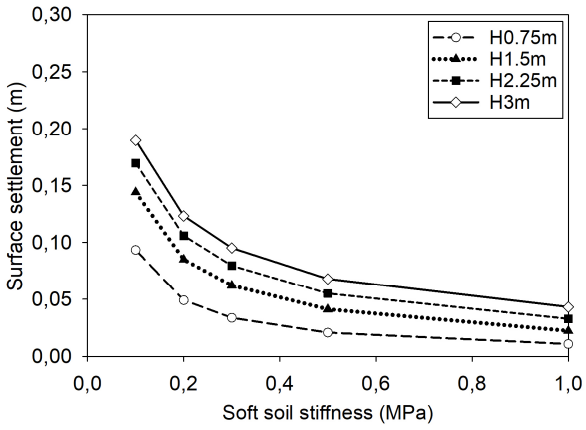


**Figure 34 Surface settlement of loose materials in FDM model (liner element)**

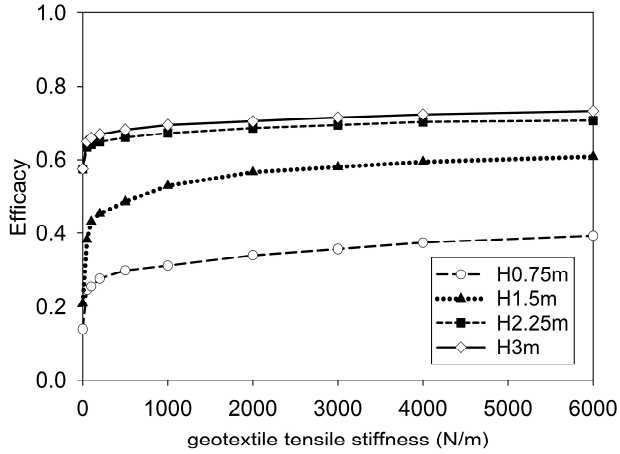


**Figure 35 Effect of geotextiles tensile stiffness in DEM model for dense granular materials**

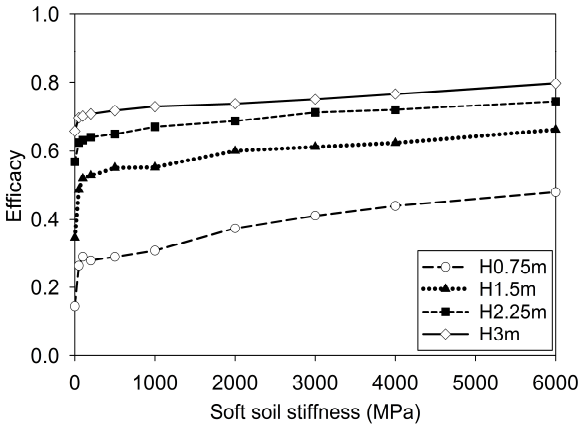


**Figure 36 Effect of geotextiles tensile stiffness in FDM model (liner element) for dense granular materials**

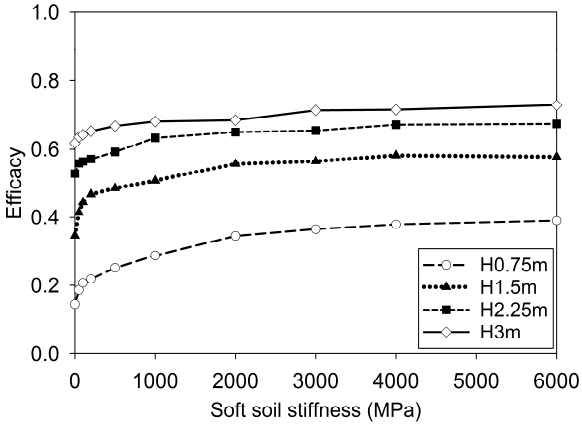


**Figure 37 Effect of geotextiles tensile stiffness in FDM model (geogrid element) for dense granular materials**

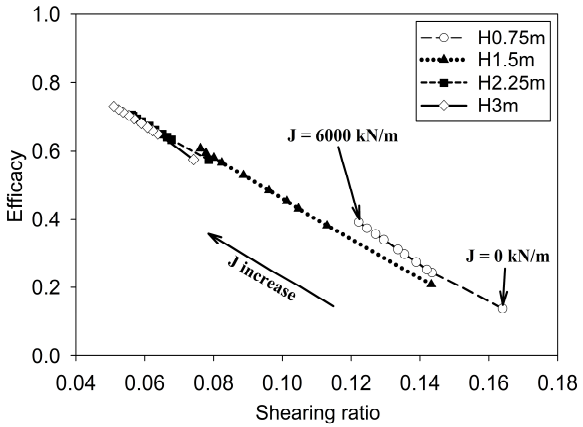


**Figure 38 Efficacy versus shearing ratio in DEM model for dense granular materials**

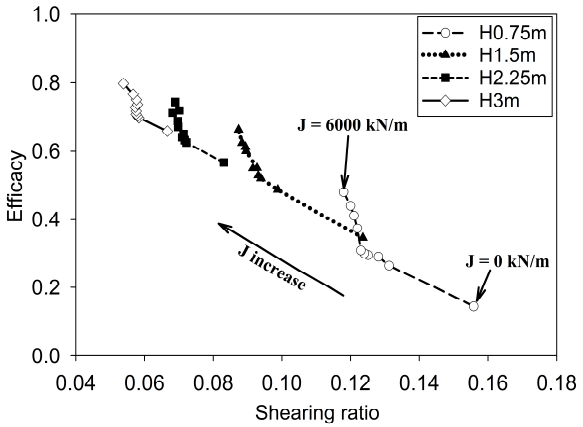


**Figure 39 Efficacy versus shearing ratio in FDM model (liner element) for dense granular materials**

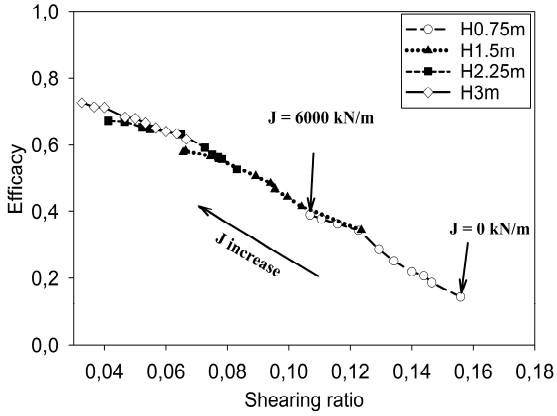


**Figure 40 Efficacy versus shearing ratio in FDM model (geogrid element) for dense granular materials**

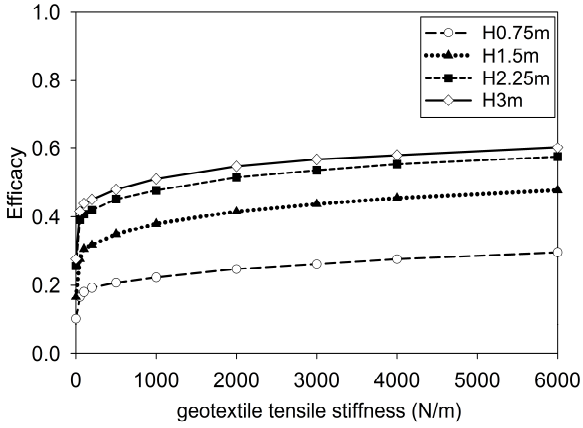


**Figure 41 Effect of geotextiles tensile stiffness in DEM model for loose granular materials**

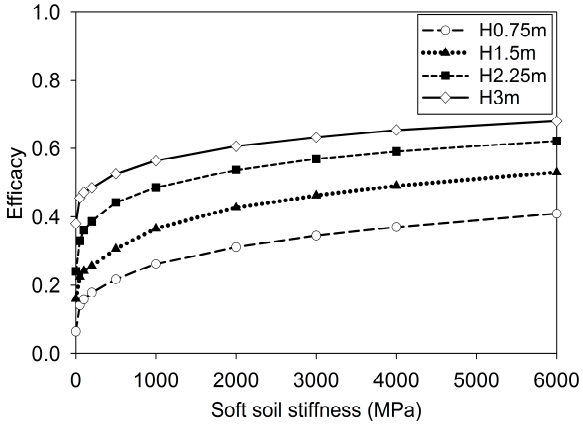


**Figure 42 Effect of geotextiles tensile stiffness in FDM model (liner element) for loose granular materials**

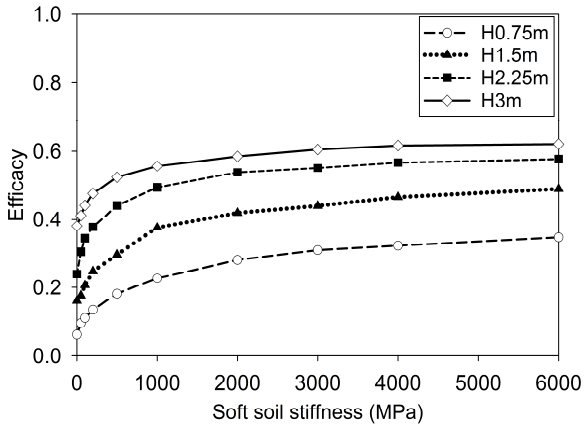


12 **Figure 43 Effect of geotextiles tensile stiffness (geogrid element) in FDM model for loose**
13 **granular materials**

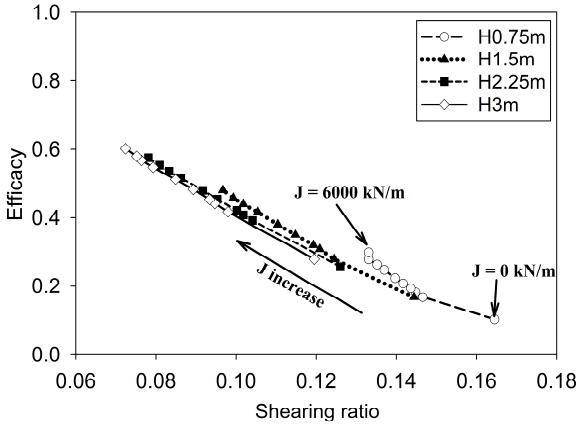


**Figure 44 Efficacy versus shearing ratio in DEM model for loose granular materials**

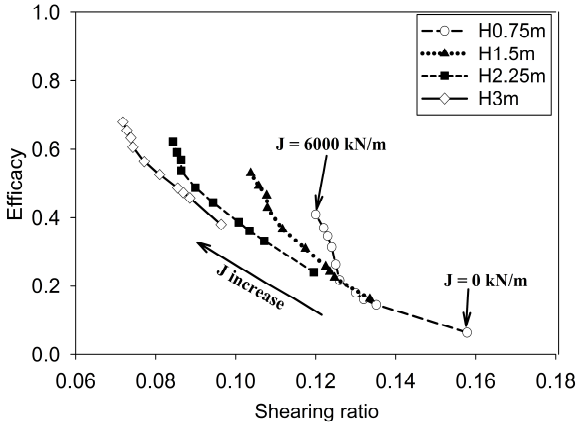


**Figure 45 Efficacy versus shearing ratio in FDM model (liner element) for loose granular materials**

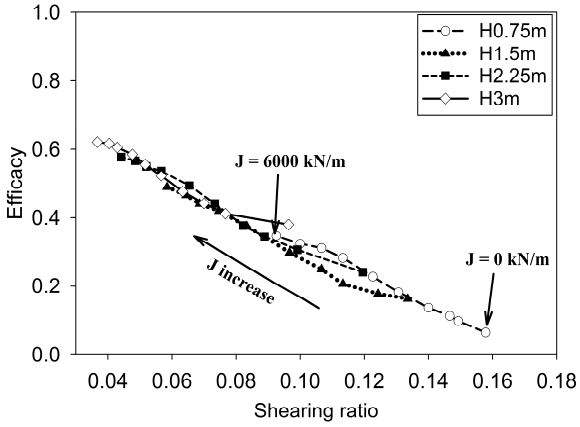


14 **Figure 46 Efficacy versus shearing ratio in FDM model (geogrid element) for loose gran-**
15 **ular materials**

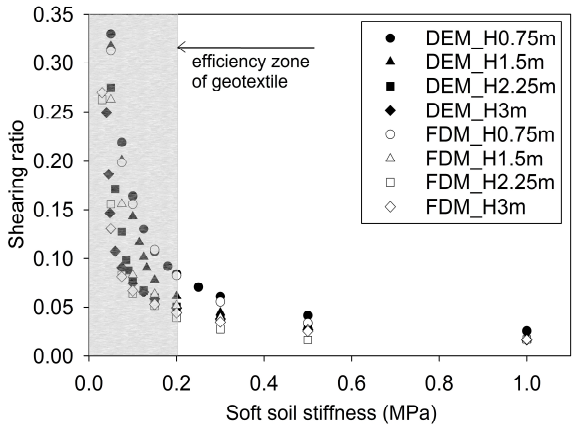


16 **Figure 47 Efficacy zone of geotextiles**

**Table 1. Micro-parameters in the DEM model for granular materials**

| Samples | Numerical Porosity | $K_n$ ($MN/m^2$) | $k_n/k_t$ | $\phi$ |
|---|---|---|---|---|
| Loose (L) | 0.41 | 10 | 1 | 40º |
| Medium (M) | 0.38 | 10 | 1 | 40º |
| Dense (D) | 0.34 | 10 | 1 | 40º |

**Table 2. Interpretation of macro-parameters from the DEM model**

| Sample | $\phi_p$(degrees) | $\phi_{cs}$(degrees) | m |
|---|---|---|---|
| Loose (L) | 34 º | 26 º | 0.36 |
| Medium (M) | 40 º | 26 º | 0.36 |
| Dense (D) | 46 º | 26 º | 0.36 |

**Table 3. Macro-parameters in the FDM model**

| Sample | $E^e_{ref}$ (MN/m$^2$) | $p_{ref}$ (kPa) | υ | m | $\phi_p$ (degree) | $\phi_{cs}$ (degree) | $R_f$ | β | $h_\phi$ (degree) | $e_o$ | Volumetric weight (kg/m$^3$) |
|---|---|---|---|---|---|---|---|---|---|---|---|
| Loose | 100 | 100 | 0.2 | 0.36 | 34° | 26° | 0.9 | 0.12 | 250° | 0.7 | 1470 |
| Medium | 120 | 100 | 0.2 | 0.36 | 40° | 26° | 0.9 | 0.12 | 250° | 0.61 | 1550 |
| Dense | 160 | 100 | 0.2 | 0.36 | 46° | 26° | 0.9 | 0.12 | 250° | 0.51 | 1650 |

| | | | |
|---|---|---|---|
| $E^e_{ref}$ | Reference Young's modulus | $\phi_{cs}$ | Critical state friction angle |
| $p_{ref}$ | Reference mean stress | $R_f$ | Failure ratio constant |
| υ | Poisson's ratio | β | Calibration factor |
| m | Stress dependence constant | $h_\phi$ | Softening friction angle |
| $\phi_p$ | Peak friction angle | $e_o$ | Initial void ratio |

**Table 4. Numerical calibration of geotextile in discrete and continuum model**

| DEM | FDM | |
|---|---|---|
| J (kN/m) | thickness t (m) | Young's modulus E(MN/m$^2$) |
| 50 | 0.01 | 8.33 |
| 100 | 0.01 | 16.66 |
| 200 | 0.01 | 33.33 |
| 500 | 0.01 | 83.33 |
| 1000 | 0.01 | 166.66 |
| 2000 | 0.01 | 333.33 |
| 3000 | 0.01 | 500 |
| 4000 | 0.01 | 666.66 |
| 6000 | 0.01 | 1000 |